 CMC, vol.37, no.3, pp.161-193, 2013

From Ordered to Disordered: The Effect of Microstructure on Composite Mechanical Performance

L.B. Borkowski[1], K.C. Liu and A. Chattopadhyay

Abstract: The microstructural variation in fiber-reinforced composites has a direct relationship with its local and global mechanical performance. When micromechanical modeling techniques for unidirectional composites assume a uniform and periodic arrangement of fibers, the bounds and validity of this assumption must be quantified. The goal of this research is to quantify the influence of microstructural randomness on effective homogeneous response and local inelastic behavior. The results indicate that microstructural progression from ordered to disordered decreases the tensile modulus by 5%, increases the shear modulus by 10%, and substantially increases the magnitude of local inelastic fields. The experimental and numerical analyses presented in this paper show the importance of microstructural variability when small length scale phenomena drive global response.

Keywords: Microstructures, mechanical property variation, material uncertainty, computational mechanics, micromechanics.

1 Introduction

Micromechanics-based modeling approaches have been used extensively in the past and have been shown to provide accurate results with limited computational effort [Kanouté et al. (2009)]. Many of these approaches assume a periodic arrangement of fibers, such as square or hexagonal packing sequences, as an approximation to a complex problem. Experimental micrographs of composite microstructure, such as those seen in Fig. 1, have shown that actual microstructures in polymer matrix composites rarely resemble ordered arrangements and show at least some degree of spatial randomness. Therefore, researchers have studied the generation of random microstructures and microstructures that are statistically equivalent to experimental microstructures [Gusev, Hine, and Ward (2000); Byström (2003); Wongsto and Li (2005); Melro, Camanho, and Pinho (2008); Wang et al. (2011); Liu and Ghoshal

[1] ASU, Tempe, AZ, 85287, U.S.A.

(2013a)]. In addition, there has been a complimentary focus on quantifying the necessary size of the representative volume element (RVE) that is able to accurately capture the behavior of the ‘random’ composite as a whole [Drugan and Willis (1996); Gusev (1997); Ostoja-Starzewski (1998); Shan and Gokhale (2002); Kanit et al. (2003); Trias et al. (2006)]. In Smit, Brekelmans, and Meijer (1999) it is postulated that the only means to accurately capture the inelastic macroscopic behavior of a microstructure, caused by the initiation and progression of plastic flow, is to represent the position of inclusions as random variables. Microstructural variability is ignored when the models assumed an ordered array of fibers. Depending on the analysis length scale, these models assuming ordered arrays of fibers or particles have various degrees of accuracy in simulating global composite behavior, while the predictive capability of the models typically improves with increasing length scales [Terada et al. (2000); Swaminathan, Ghosh, and Pagano (2006)]. For purely elastic analysis, as the scale of interest increases to the structural, the unidirectional composite can be regarded as a transversely isotropic and homogeneous material with reasonable accuracy [Reddy (1987)]. The diminishing effect of microscale randomness at higher length scales can be expected for monotonic loading conditions and is one reason that the models utilizing the assumption of ordered fiber arrays or homogeneous transversely isotropic properties have provided reasonable results in the past as long as local inelastic phenomena (e.g, plasticity or damage initiation) are not prevalent.

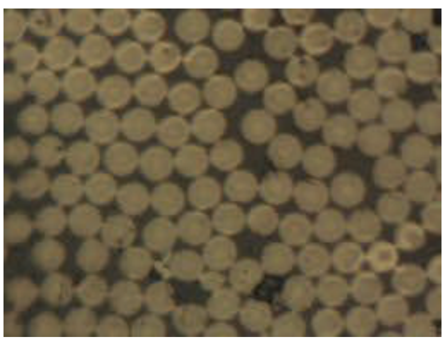

Figure 1: Micrograph of polymer matrix composite at 1000X magnification

Researchers have investigated the effect of random or disordered microstructures on various composite behavior, including elastic and damage [Trias et al. (2006); Huang, Jin, and Ha (2008); Maligno, Warrior, and Long (2009); Wang et al. (2011); Romanov et al. (2013)]. Wang et al. (2011) and Trias et al. (2006) focused on the generation of random distributions of fibers and quantified its elastic and failure effect using a two dimensional (2D) RVE finite element method (FEM) model loaded in transverse tension. Their results indicate that as the disorder in the microstructure increases the tensile modulus will also increase; the authors concluded that this phenomenon is caused by the higher fiber stresses in the random microstructure when compared to the ordered microstructure. Huang, Jin, and Ha (2008) developed a three dimensional (3D) RVE model for the purpose of studying the effects of transverse tensile, shear, and thermal loading on the elastic behavior (e.g., traction, stress concentration, and stress invariant distributions) for ordered and random microstructures of varying volume fractions and loading angles. One conclusion the authors reached is that the range in stress invariant distribution is wider for a random fiber array compared to an ordered array due to irregularity in interfiber distance, which results in lower predicted strength. Maligno, Warrior, and Long (2009) investigated the local elastic and damage evolution effects of interfiber spacing in unidirectional fiber-reinforced composites using an RVE comprised of three partial fibers. The authors found that the interfiber spacing and residual stress play an important role in damage initiation and evolution. Romanov et al. (2013) verified that the heuristic random microstructure generation (RMG) algorithm [Melro, Camanho, and Pinho (2008)] was capable of creating microstructures that are statistically equivalent to real fiber distributions. Liu and Arnold (2013) investigated the effects of varying microstructures in ceramic matrix composites and determined that the effect of randomness diminishes as length scale increases for elastic and damage phenomena. Heterogeneous microstructures containing inclusions, voids, and cracks with regular as well as arbitrary geometries were directly modeled using Trefftz Computation Grains, T-Trefftz Voronoi Cell Finite Elements, and SGBEM Voronoi Cells in Dong, Gamal, Atluri (2013), Dong and Atluri (2012), and Dong and Atluri (2013) respectively. Accurate and computationally efficient modeling techniques were developed by the authors to demonstrate how geometric and material property randomness propagates to the macroscale, thereby affecting the stochastic global response of the composite.

In this paper, a micromechanics-based model is developed to represent the relationship between the microstructural variation and the macroscale behavior of a unidirectional composite. The authors attempt to address and quantify a fundamental issue in composite materials: what the effect of microstructural spatial variation on the macroscopic elastic and inelastic composite behavior is. Simulations were conducted starting with a 3D composite RUC with an ordered microstructure (i.e., square fiber packing) for tensile and shear loading conditions. For each subsequent simulation the fiber positions were perturbed randomly resulting in a less ordered configuration. This process was carried out until the microstructure was completely random (i.e., complete spatial randomness of fibers). It is concluded that as a microstructure progresses from ordered to disordered, local and global RUC fields (elastic and inelastic) evolve at different rates, promoting variation in scale-dependent behavior. Furthermore, the authors investigate whether the variation in global composite properties, due to the increasing disorder of the microstructure, is significant. This investigation indicates that the effect of the disorder is more significant at the small length scales and becomes less significant at the continuum homogeneous level. Although little effect of microstructural randomness may be evident at the macroscale, local fields are greatly affected by changes in fiber spacing and arrangement. Accurately capturing the local fields is important when inelastic or damage behavior initiation and progression is of interest at the microscale. With increased loading at low strain rates, the effect of microscale inelastic behavior becomes more pronounced at the macroscale, potentially meriting consideration of microscale disorder for macroscale simulations. Studies demonstrating the statistical equivalence between experimental micrographs and simulated microstructures in addition to simulations indicating the similarity in elastic and inelastic behavior for statistically equivalent microstructures provide validation for the studies carried out in the present article.

2 Micromechanics Modeling of Unidirectional Fiber Variability

Micromechanics approaches can be utilized to capture the global behavior, both elastic and inelastic, of heterogeneous structures as a function of its constituent materials and microstructure. In unidirectional, fiber-reinforced composites, the fluctuation in the micro-stresses and micro-strains due to the interaction between the constituents must be explicitly accounted for in order to accurately capture the local and global behavior of the composite system. Local information is lost in macroscopic approaches utilizing homogenization techniques to simplify the analysis, especially when the microstructure contains spatial variation that causes its behavior to differ from that of an ordered microstructure. Additionally, micromechanics-based models allow for the identification of inelastic and failure behavior in the individual composite constituents. For the analyses of heterogeneous microstructures, 3D mechanics models have been shown to more accurately represent the complex stress and strain distributions, particularly in the vicinity of inclusions [Danielsson, Parks, and Boyce (2002); Krueger et al. (2002)]. Simplifications of the 3D problem to 2D, utilizing plane stress or plane strain assumptions, ease the complexity of analysis while still providing qualitative global deformation and stress behavior. Two dimensional idealizations of the 3D microstructure provide realistic predictions of macroscopic stress/strain behavior for low volume fractions of inclusions [Socrate and Boyce (2000)]; however, for greater volume fractions the inclusions can no longer be assumed isolated, and the 2D simplifications fail to provide accurate predictions of the stress and strain states in the vicinity of the inclusions [Danielsson, Parks, and Boyce (2002)]. Additionally, in composites containing constituents whose mechanical properties differ, in particular for those that differ greatly, 2D models fail to capture the complex localized kinetic and kinematic behavior near the inclusion/matrix interface [Krueger et al. (2002); Chawla and Chawla (2006)]. Although greater computational resources are required for full 3D analyses, comparisons with experiments have demonstrated their improved accuracy over those assuming a 2D stress or strain state [Chawla and Chawla (2006)].

A full 3D model of the unidirectional cross section will be simulated in order to capture the inelastic behavior that often initiates at the fiber/matrix interface, resulting in the accurate prediction of stress and strain states in this region of fundamental importance. Triply periodic boundary conditions are imposed on the composite microstructure RUC where periodicity is enforced for the displacement degrees of freedom at the boundary nodes in the three coordinate directions. Although the imposition of periodic boundary conditions for microstructure unit cells may seem artificial based on visual inspection of experimental micrographs (Fig. 1), numerical and theoretical analyses have been conducted by Terada et al. (2000) and Sab (1992) respectively, demonstrating that periodic conditions are well suited for the representation of disordered composite microstructures using micromechanical analysis techniques.

2.1 Development of 3D RUC Finite Element Model

A unidirectional carbon fiber composite lamina was modeled using the commercial FEM software Abaqus/Standard. An FEM model was chosen in this case because semi-analytical methods may have inherent ambiguity when modeling random microstructures [Liu and Ghoshal (2013b)]. The 3D, triply periodic RUC with a fiber volume fraction of 52.5% includes 100 fibers and has a depth (i.e., thickness) of a single element. Investigation of experimental microstructures using statistical descriptors, such as Ripley's K-function [Ripley (1977)] and the two-point correlation function [Torquato (2001)], has shown that approximately 100 fibers are required within an RVE for convergence within a 5% deviation [Liu and Ghoshal (2013a)]. The fiber center positions were determined using an algorithm that begins with an ordered square packing arrangement and then randomly perturbs the positions of each of the fibers. If the motion of a fiber causes it to interfere with another fiber then that motion is rejected and another is attempted, thereby satisfying the requirements of the hard-core model where fibers have an equal likelihood of residing anywhere in the domain except where other fibers currently reside. Additionally, if a portion of a fiber cross section passes over the boundary of the RUC, that portion is redrawn on the opposite side of the RUC in order to satisfy periodic boundary conditions. For each microstructure created, the coordinates of the fiber positions were saved and various statistical measures were used to quantify the randomness of the microstructure. Fiber position Monte Carlo perturbations were carried out until the statistical measures indicated that the simulated microstructure could be classified as a hard-core model. Further details of the statistical characterization techniques are provided in Section 2.3.

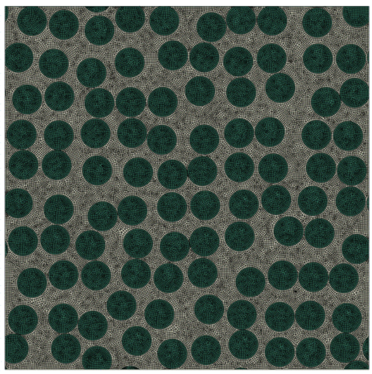

Figure 2: Meshed FEM microstructural model

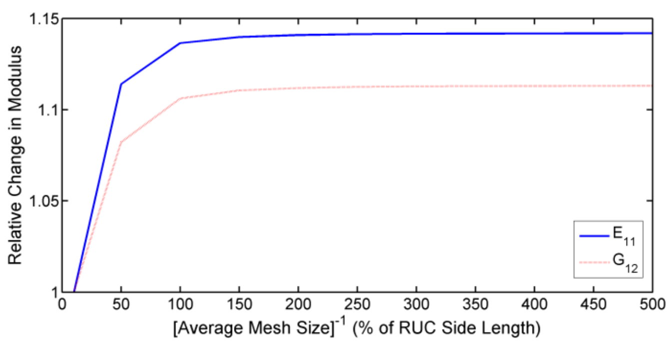

Figure 3: Mesh convergence analysis

The meshed microstructural FEM model is shown in Fig. 2. Each fiber is meshed with approximately 57 nodes around its circumference. The composite RUC mesh is comprised of a combination of 6-node linear triangular prism and 8-node linear brick elements and a seed size of 0.5% of the total RUC edge length was used based on results from a convergence analysis presented in Fig. 3. Values for the transverse elastic tensile and shear moduli were found to obtain approximately 90% of their respective convergent values at this element size, which was deemed sufficient for the sake of computational efficiency. A swept mesh technique was used to ensure that the element nodes on the front and back of the 3D RUC coincide, which is necessary for assigning kinematic constraints enforcing periodicity in the composite through-thickness direction. The PR520 epoxy resin matrix material was modeled as homogeneous and isotropic, and the T300 carbon fibers were modeled as transversely isotropic. The material properties of the matrix and fiber materials are shown in Tab. 1.

Table 1: Constituent material properties

Constituent	T300	PR520
E_{11} (GPa)	231.0	3.35
E_{22} (GPa)	22.4	—
G_{12} (GPa)	15.0	—
ν_{12}	0.3	0.38
ν_{23}	0.35	—

A perfect bond was assumed between the fiber and matrix since interfacial effects, such as fiber debonding, was not a focus and therefore not investigated in this study. The elastic behavior of the matrix and fiber materials was modeled using a linear elastic constitutive relation, while the inelastic behavior of the matrix material was modeled using a strain rate dependent viscoplastic associative flow formulation described in Section 2.2. The matrix was modeled as elastic and elastic/viscoplastic in separate analyses to investigate the effect of fiber spatial variation on the local and global composite behaviors under various loading conditions and strain rates.

The 3D RUC periodic boundary conditions were enforced using the technique described in Danielsson, Parks, and Boyce (2002) and implemented within Abaqus through the use of linear constraint equations. With this technique, three fictitious reference nodes are introduced and their nine total displacement degrees of freedom, represented by ξ_i for i=1 to 9, are related to the components of the macroscopically applied deformation gradient $\mathbf{F}$, as seen in Eq.1.

$$\begin{bmatrix} \xi_1 & \xi_2 & \xi_3 \\ \xi_4 & \xi_5 & \xi_6 \\ \xi_7 & \xi_8 & \xi_9 \end{bmatrix} = \begin{bmatrix} (F_{11}-1) & F_{12} & F_{13} \\ F_{21} & (F_{22}-1) & F_{23} \\ F_{31} & F_{32} & (F_{33}-1) \end{bmatrix} \tag{1}$$

The principle of virtual work, Eq.2, can be expressed as in Eq.3 where V_0 is the volume in the reference configuration, **S** is the first Piola-Kirchhoff stress tensor, $\tilde{s}$ is the surface traction in the reference configuration, δu is the virtual displacement, and S_0 is the surface area in the reference configuration.

$$\delta W^{int} = \delta W^{ext} \tag{2}$$

$$V_0 \boldsymbol{S} \cdot \delta \boldsymbol{F} = \int_{S_0} \tilde{\boldsymbol{s}} \cdot \delta \boldsymbol{u} dS_0 \tag{3}$$

The external work may be expressed in terms of the generalized nodal degrees of freedom, ξ_i, and their work conjugate generalized forces, Ξ_i, as seen in

$$\delta W^{ext} = \sum_{i=1}^{9} \Xi_i \delta \xi_i \tag{4}$$

Hence in the FEM framework, the components of Ξ are the reaction forces of the reference nodes. The components of the macroscopic first Piola-Kirchhoff stress tensor, **S**, can be written as a function of the reaction forces as

$$\begin{bmatrix} S_{11} & S_{12} & S_{13} \\ S_{21} & S_{22} & S_{23} \\ S_{31} & S_{32} & S_{33} \end{bmatrix} = \frac{1}{V_0} \begin{bmatrix} \Xi_1 & \Xi_2 & \Xi_3 \\ \Xi_4 & \Xi_5 & \Xi_6 \\ \Xi_7 & \Xi_8 & \Xi_9 \end{bmatrix} \tag{5}$$

Finally the components of the Cauchy stress tensor are computed using the following relationship

$$\boldsymbol{\sigma} = \frac{V_0}{V} \boldsymbol{S} \boldsymbol{F}^T \tag{6}$$

where V is the volume in the current configuration.

The technique of imposing periodic boundary conditions by defining linear constraint equations in the Abaqus input file constrains the degrees of freedom of the boundary nodes residing on opposite sides of the RUC to the specified displacement of one of the three reference nodes. For example, assuming nodes 1 and 101 are corresponding nodes on opposites sides of the 3D RUC, their relative displacement components can be defined with respect to the displacement of reference node R_1 using the following equations

$$\begin{aligned} u_1^1 - u_1^{101} - u_1^{R_1} &= 0 \\ u_2^1 - u_2^{101} - u_2^{R_1} &= 0 \\ u_3^1 - u_3^{101} - u_3^{R_1} &= 0 \end{aligned} \tag{7}$$

where the subscript on u denotes the constrained degree of freedom and the superscript designates the node number or identification. Degrees of freedom 1, 2, and 3 correspond to displacement along the three Cartesian axes. Similar equations are defined for each corresponding node pair on opposite sides of the RUC, thereby tying their degrees of freedom to those of the reference nodes R_1, R_2, and R_3. Using this framework, the loading conditions of the entire composite can be prescribed by simply imposing conditions on the degrees of freedom of the three reference nodes. A representative illustration of the position of the three reference nodes is presented in Fig. 4. For further details regarding the application of linear constraint equations the reader is directed to the Abaqus documentation [Abaqus (2009)].

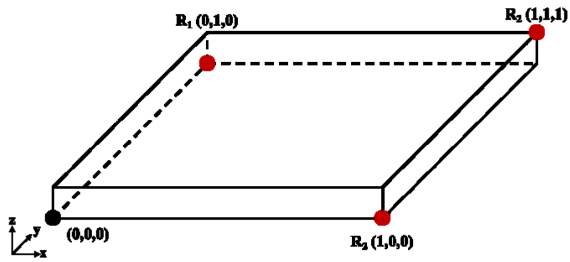

Figure 4: Representation of reference node positions

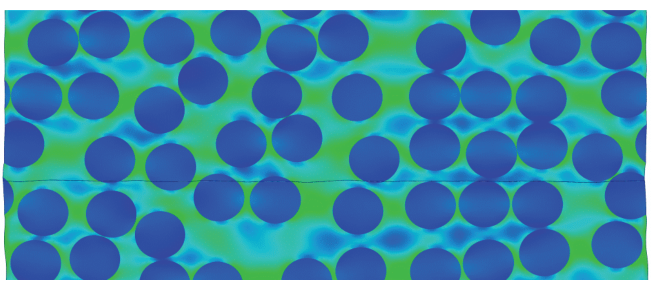

Figure 5: Kinematic periodicity in RUC

To verify that periodicity in the kinematic degrees of freedom is properly enforced in the developed FEM model, the deformed contour of maximum principal strain is plotted for an RUC with a hard-core fiber distribution and is patterned vertically to compare the bottom and top edges of the RUC for continuity, as seen in Fig. 5. The match in the deformed edge shape provides validation that the displacements are periodic, while the continuity in strain contours provides a qualitative check for periodicity. Patterned contours of the kinematic and kinetic field variables were created in the remaining two coordinate directions to check for periodicity with similarly satisfactory results. The triply periodic micromechanics-based FEM model can now be used to represent the global and local composite behavior as a function of constituent geometric, architectural, and material properties.

2.2 Rate Dependent Inelasticity Consideration

The local effects of micro-stresses and micro-strains due to the random arrangement of fibers in PMCs can be accounted for through the use of inelastic constitutive models. In previous studies examining the local effect of non-uniform fiber distributions [Trias et al. (2006); Huang, Jin, and Ha (2008); Maligno, Warrior, and Long (2009); Wang et al. (2011)] researchers have attempted to quantify the variation in inelastic matrix behavior through comparisons of stress invariant, energy, and traction distributions. While this information may provide reasonable estimates of yield onset, it does not account for inelastic behavior progression, load redistribution, and rate dependence occurring throughout the loading process. Since polymer epoxies commonly used for PMCs generally obey rate-dependent plastic constitutive relations, inelastic models based on viscoplasticity theory have been observed to capture the response of these materials [Goldberg, Roberts, and Gilat (2005)]. Incorporating viscoplastic constitutive laws within a micromechanics model allows for the variation in matrix inelastic behavior to be mapped not only to the initiation time and location, but also provides the ability to capture the variation's effect on inelasticity propagation and concentration. These phenomena can also be investigated with respect to loading rate and type.

Previously, researchers have established that polymers used in composite applications exhibit a nonlinear rate dependent constitutive response with hydrostatic driven yield function [Pae and Mears (1968); Rabinowitz, Ward, and Parry (1970); Pugh et al. (1971); Wronski and Pick (1977); Ward and Sweeney (2012)]. Goldberg, Roberts, and Gilat (2005) used a viscoplastic constitutive model with an associative flow rule including hydrostatic stress effects, implemented within a micromechanics framework, to capture the nonlinear behavior of polymer matrix composite material systems loaded at low to high strain rates (e.g., 5E-5/s to 400/s). The viscoplastic constitutive model provided accurate results for both monolithic (i.e., neat) polymer and continuous fiber-reinforced composite experimental specimens throughout the low to high strain rate range. Due to its proven accuracy, this constitutive model was implemented into the micromechanics model to predict the inelastic material behavior of the matrix constituent. In the viscoplastic constitutive model formulation, the inelastic potential function is defined based on the

Drucker-Prager yield criterion,

$$f = \sqrt{J_2} + \alpha\sigma_{kk} \tag{8}$$

where J_2 is the second invariant of the deviatoric stress tensor, α is a state variable that controls the level of hydrostatic stress effects, and σ_{kk} is the first invariant of the stress tensor. The second term in Eq.8 incorporates the effect of hydrostatic stress into the potential function. The final inelastic strain rate expression is

$$\dot{\varepsilon}^I_{ij} = 2D_0 \exp\left[-\frac{1}{2}\left(\frac{Z}{\sigma_e}\right)^{2n}\right]\left(\frac{S_{ij}}{2\sqrt{J_2}} + \alpha\delta_{ij}\right) \tag{9}$$

where D_0 and n are material parameters, Z is a state variable that represents the resistance to internal stress, S_{ij} are the components of the deviatoric stress tensor, δ_{ij} is the Kronecker delta, and σ_e is the effective stress expressed in terms of the yield function as

$$\sigma_e = \sqrt{3}f \tag{10}$$

The evolution rate of the internal state variables Z and α are expressed as

$$\dot{Z} = q\,(Z_1 - Z)\,\dot{e}^I_e \tag{11}$$

and

$$\dot{\alpha} = q\,(\alpha_1 - \alpha)\,\dot{e}^I_e \tag{12}$$

where $\dot{e}^I_e$ is the effective deviatoric inelastic strain rate, which can be written as

$$\dot{e}^I_e = \sqrt{\frac{2}{3}\dot{e}^I_{ij}\dot{e}^I_{ij}} \tag{13}$$

where

$$\dot{e}^I_{ij} = \dot{\varepsilon}^I_{ij} - \dot{\varepsilon}^I_m\delta_{ij} \tag{14}$$

The rate dependent viscoplasticity model was implemented into the FEM micromechanics model via a user material subroutine (UMAT) in Abaqus/Standard to be called at each matrix integration point during the loading process. The epoxy matrix (PR520) material parameters for the viscoplasticity model are provided in Tab. 2, and details regarding the experimental determination of each parameter can be found in Goldberg, Roberts, and Gilat (2005).

Table 2: Material parameters for viscoplasticity model

	D_0 $(1/s)$	n	Z_0 (MPa)	Z_1 (MPa)	q	α_0	α_1
PR520	1x10^6	0.93	396.09	753.82	279.26	0.568	0.126

2.3 Generation and Quantification of Microstructural Variability

When simulating microstructures to match experimental materials, several statistical criteria have to be satisfied in order for the simulation to be validated. A set of criteria was presented in Liu and Ghoshal (2013a) to determine the validity of a simulated microstructure. In this paper the authors assume that composite microstructures follow a hard-core distribution and use Monte Carlo perturbation to achieve a final arrangement starting with an initially ordered array. Various point processes can be used as statistical parameters to characterize experimental and numerically generated microstructures. Two such processes that are often used to provide qualitative assessment of the randomness of fibers distributed in a matrix cross section are the Ripley's K-function and the pair distribution function. In this analysis, these two functions are called upon to determine whether various generated and experimental microstructures are statistically equivalent and to quantify their degree of randomness. Ripley's K-function [Ripley (1977)] is given by

$$K(r) = \frac{A}{N^2} \sum_{k=1}^{N} w_k^{-1} I_k(r) \tag{15}$$

where A is the domain area, N is the number of fibers within the domain area A, w_k is the proportion of the circumference of radius r within area A to the total circumference of radius r, and I_k(r) is the number of fiber centers within the sampling area with radius r. The pair distribution function g(r) [Pyrz (1994)] describes the probability of additional fiber centers falling within the area formed by inner radius r and outer radius $r+dr$ and can be expressed as a function of Ripley's K-function by

$$g(r) = \frac{1}{2\pi r} \frac{dK(r)}{dr} \tag{16}$$

Given that the convergence of the K-function can provide information regarding the progression of an ordered microstructure to one that can be described as hard-core, the authors may use this point process to verify the randomness of simulated microstructures (e.g., Fig. 6) created using the previously described Monte Carlo perturbation technique. Each of the three microstructures (ordered, semi-random, and hard-core) contains 100 fibers and periodicity of the fibers is enforced at the

RUC boundaries. Fig. 7 presents the K-function for the three generated microstructures. Convergent behavior of the K-function can be observed as the microstructures approach a hard-core distribution, evident by the reduction in discrete steps and subsequent smoothing of the K-function. An initial step is seen in the K-function of the semi-random and hard-core microstructures. The presence of this step indicates the existence of local order at small values of r/r_m. Previous studies have concluded that this initial step becomes more pronounced as the fiber volume fraction increases, while for fiber volume fractions below approximately 50% the step is minimal or nonexistent [Liu and Ghoshal (2013a)].

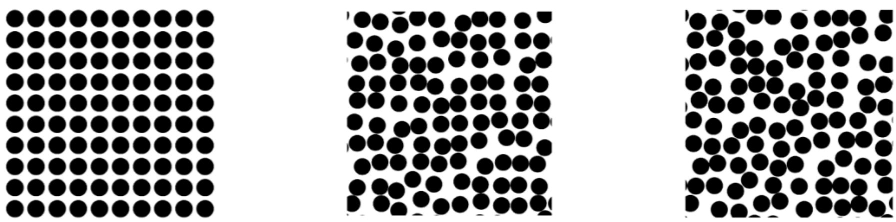

(a) Ordered (b) Semi-random (c) Hard-core

Figure 6: Simulated microstructures generated using a Monte Carlo perturbation framework

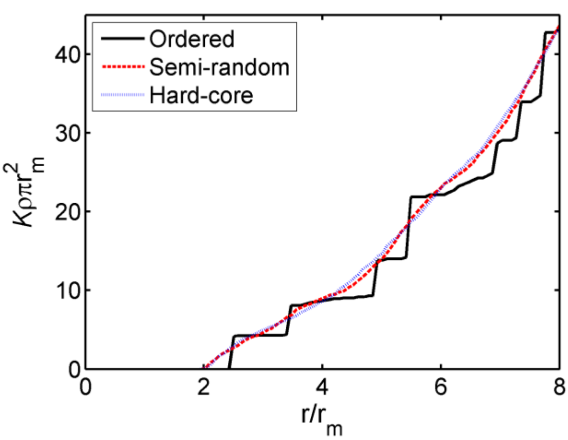

Figure 7: Ripley's K-function for three simulated microstructures

Experimental micrographs, such as Fig. 1, demonstrate the existence of variation in fiber diameter as well as variation in position. Utilizing image processing techniques, a probability distribution function can be created to represent the fiber diameter variation in the experimental microstructure using either the Feret diameter or diameter from inclusion area techniques. The Feret diameter (defined as the maximum distance between any two points on a fiber's boundary) and the diameter from inclusion area (defined as the circle diameter required to represent the equivalent inclusion area) were calculated for each fiber and their normal distribution fits are shown plotted in Fig. 8. Due to the presence of microstructure defects and polishing damage seen in Fig. 1, the mean fiber diameter predicted using the latter approach is underestimated since these damage artifacts are interpreted as matrix by the image processing software. Therefore for this case (i.e., aligned fibers with circular cross sections) the Feret diameter was determined to better represent the actual fiber diameter distributions. For the experimental data, a 7% standard deviation of fiber diameters is obtained. This random architectural information will be used to investigate the effects of fiber radius in comparison with fiber position on the global composite elastic properties under tensile and shear loading conditions.

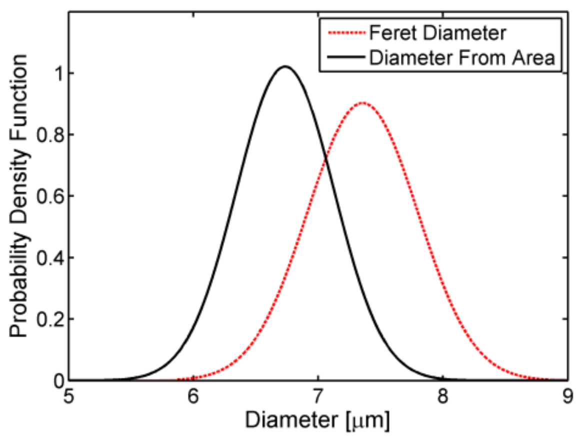

Figure 8: Probability density functions for experimental micrograph fiber diameter measurements

3 Results and Discussion

3.1 Global Elastic Behavior

To quantify the effect of microstructure disorder on elastic properties, the authors predicted the transverse tensile and shear moduli as the RUC was perturbed from ordered to complete spatial randomness. For this analysis the constituent materials were assumed to behave linearly elastic. The RUC was comprised of 100 fibers initially in a square packed array and modeled in Abaqus/Standard as triply periodic. The microstructure was perturbed in small steps until the $K-$function matched that of a hard-core distribution. At each step a uniaxial strain increment (e.g., $\Delta\varepsilon_{11}$ or $\Delta\varepsilon_{12}$) was applied while maintaining zero stress on the other boundaries (e.g., σ_{22}=0, etc.). The modulus was calculated with the traditional method (e.g., $\sigma_{11}/\varepsilon_{11}, \sigma_{12}/\gamma_{12}$). A plot of the relative change in moduli versus degree of randomness from completely ordered (i.e., square packing arrangement) to hard-core (i.e., complete spatial randomness) is presented in Fig. 9. It can be seen that as the composite microstructure becomes more disordered, the transverse tensile modulus decreases by approximately 5% while the shear modulus increases by approximately 10%. The maximum and minimum (i.e. ordered and disordered) predicted tensile moduli, 8.15 and 7.74 GPa respectively, were checked using the inverse rule of mixtures to ensure the values remain above the lower bound (6.05 GPa) for transverse tensile loading perpendicular to the fiber axes. It is hypothesized that the increase in shear modulus is caused by a more complex and lengthy load transfer path through the RVE and that the decrease in tensile modulus is a result of the presence of resin-rich pockets in the microstructures of lesser spatial order. In other words, the change in elastic moduli is a result of the fibers carrying a lesser percentage of the load for the tensile cases and greater percentage of the load for the shear cases. This hypothesis can be quantified by plotting the ratio of volume averaged stress in the fiber to that in the matrix (σ_f/σ_m). A plot of the average stress ratio is presented in Fig. 10. This plot demonstrates the stress ratio decreasing by approximately 13.3% for the tensile case and increasing approximately 21.79% for the shear case. Similar results demonstrating the redistribution of stress as a function of microstructure disorder were obtained by Romanov et al. (2013). Therefore it is evident that the redistribution of stress between the fibers and matrix as a result of varying degrees of microstructural order plays a key role in the variance in the global elastic properties of composite RUCs as the fiber distribution progresses from ordered to hard-core.

The von Mises stress contours plotted in Figs. 11 and 12 for tensile and shear loading respectively demonstrate the progression of the local elastic fields as a function of spatial order and provide insight into the variation in global elastic moduli witnessed in Fig. 9. The most noticeable difference between the von Mises stress contour of the ordered array and those of the less ordered microstructures is the presence of high stress concentrations in areas of high fiber density. It is observed that fibers that are aligned with the loading axis exhibited a higher degree of load transfer, while those that are normal to the loading axis do not contribute signifi-

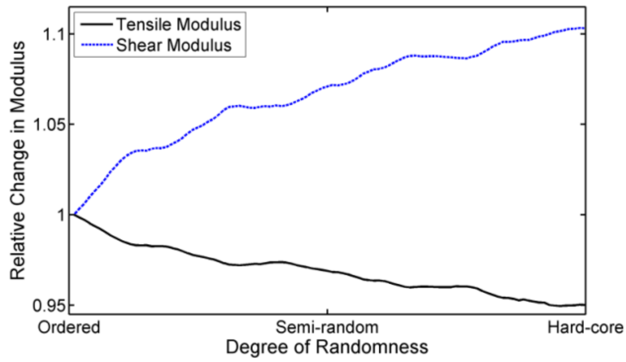

Figure 9: Global elastic moduli vs. microstructural randomness for composite RUC containing constant fiber radii

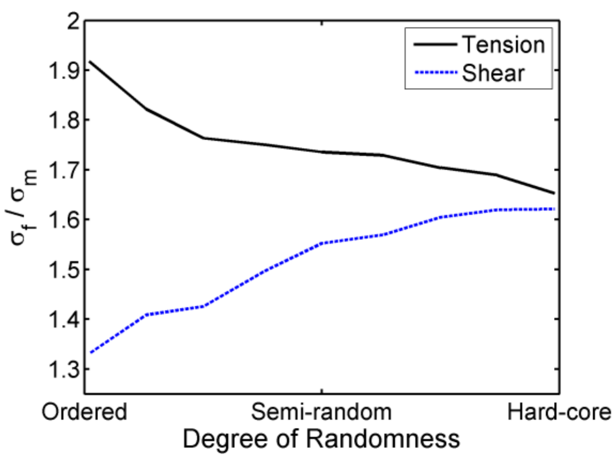

Figure 10: Volume averaged stress ratio vs. microstructural randomness

cantly to the stress distribution. Interfiber spacing is also observed playing a large role in stress concentration between and within fibers. Despite the drastic differences in von Mises stress contours between the ordered and random microstructures, little effect is observed in the elastic moduli at the global scale. Although the regions of increased stress or strain may have minimal effect on the elastic response of the composite as a whole, further investigations are necessary to quantify their effect on more local phenomena such as plasticity and failure.

The 5% decrease in tensile modulus and 10% increase in shear modulus observed in Fig. 9 may initially seem significant and merit the inclusion of microstructural variation in elastic simulations of UD composite; however, a study was conducted demonstrating whether a 5% variation in elastic material properties of the matrix and fiber has a greater or lesser effect on the global elastic properties than the random fiber positions. Experimental data of the composite constituent properties often has variation above 5% due to experimental error and inherent material property uncertainty. Additionally, process control in composite manufacturing leads to variation in matrix material properties due to variability in the cure profile (i.e., time, temperature, and pressure) and layup technique and quality. The results obtained from this study suggest that for elastic simulations of UD composites loaded in transverse tension and shear, the inherent variability in constituent properties will likely have a greater impact on the predicted global composite properties than the microstructural variability. Therefore, for the sake of model tractability there is little need to accurately represent the experimental or random nature of fiber positions if the goal is to obtain homogenized elastic properties, especially as the length scale of analysis increases.

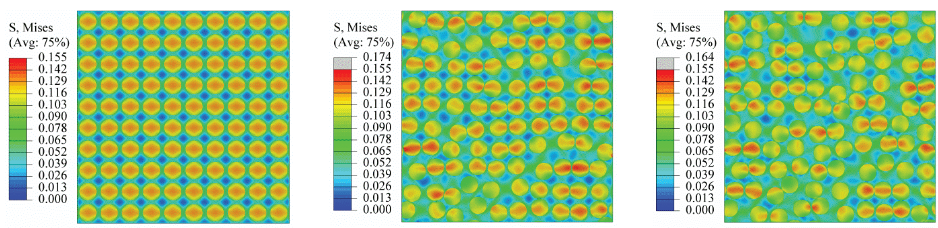

(a) Ordered microstructure

(b) Semi-random microstructure

(c) Hard-core microstructure

Figure 11: von Mises stress contour (GPa) of UD composite loaded in transverse tension

Using the fiber diameter distribution information obtained in Section 2.3, 100 microstructures were created beginning with an ordered array comprised of fibers with a random sampling of fiber diameters and using a Monte Carlo perturbation framework to increase disorder until K-function convergence was obtained. The microstructures, progressing from ordered to hard-core, were modeled in Abaqus/Standard as triply periodic RUCs and loaded similarly to the microstructures in the previous analysis with constant fiber radii. The purpose of this study is to investigate the effect of fiber geometric variation in comparison to architectural disorder in relation to global composite elastic behaviors. The predicted global tensile and shear moduli results from these simulations are presented in Fig. 13, while the von Mises stress contours are shown in Fig. 14 and Fig. 15 for tensile and shear loading

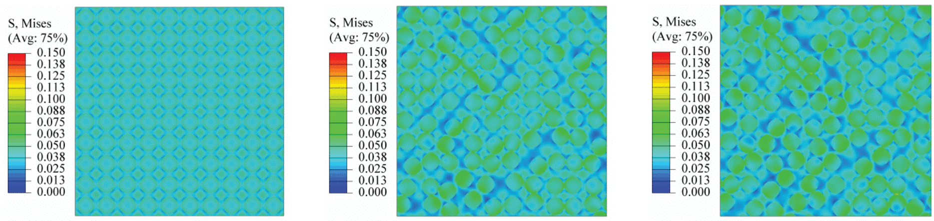

(a) Ordered microstructure (b) Semi-random microstructure (c) Hard-core microstructure

Figure 12: von Mises stress contour (GPa) of UD composite loaded in transverse shear

respectively. Through the comparison of Fig. 9 and Fig. 13 it can observed that the global elastic response of ordered to hard-core microstructures with constant and random fiber diameters demonstrate similar overall trends and final states (i.e. an approximate 5% decrease in tensile modulus and 10% increase in shear modulus). Comparison of the stress contours reveals only subtle differences, including the non-ordered distribution of stress in the ordered fiber array with varying fiber diameters. However, as presented in the previous analysis, the variation in stress concentration has little effect on global properties but may play a larger role when inelastic, local behavior is of interest. From the simulations accounting for fiber position and size variation, it can be concluded that the effect of increasing fiber position randomness has a significantly greater effect on global properties compared to the effect of fiber diameter variation. This conclusion is in agreement with the work presented in Gusev, Hine, and Ward (2000).

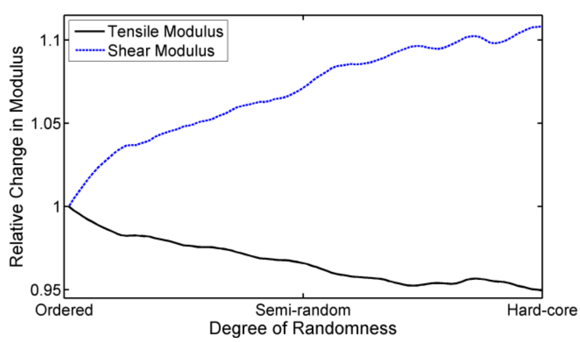

Figure 13: Global elastic moduli vs. microstructural randomness for composite RUC containing experimentally determined distribution of fiber radii

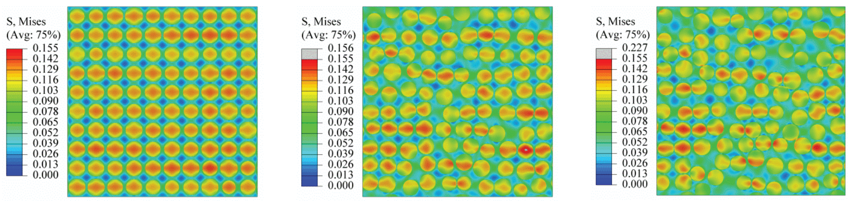

(a) Ordered microstructure (b) Semi-random microstructure (c) Hard-core microstructure

Figure 14: von Mises stress contour (GPa) of UD composite with random distribution of fiber radii loaded in transverse tension

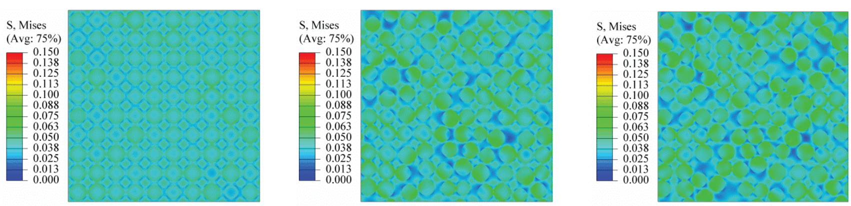

(a) Ordered microstructure (b) Semi-random microstructure (c) Hard-core microstructure

Figure 15: von Mises stress contour (GPa) of UD composite with random distribution of fiber radii loaded in transverse shear

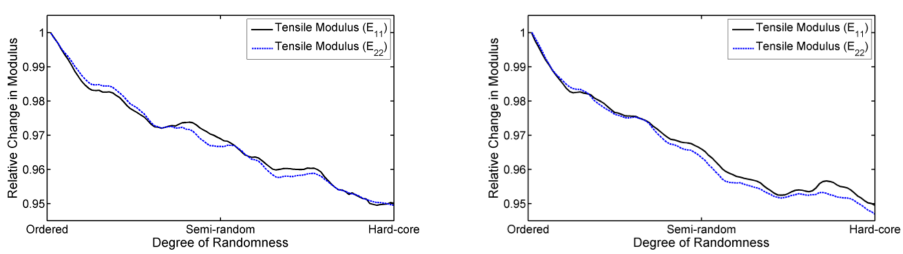

(a) Composite RUC with constant distribution of fiber radii (b) composite RUC with random distribution of fiber radii

Figure 16: Effective inelastic strain contour for ordered RUC

In the previous analyses, the progression of global tensile modulus was only presented for a single transverse direction (e.g. E_{11}). Given that the perturbation of fiber position will cause deviation from global orthotropic composite response typically assumed for ordered arrangements of fibers, a study was conducted to investigate the degree at which the elastic tensile response differs between the 'x' (i.e., 11) and 'y' (i.e., 22) transverse coordinate directions. The same 100 microstructures were loaded in tension in the 22 direction for the cases of constant and random fiber radii and the results compared to those obtain from loading in the 11 direction, as presented in Fig. 16(a) and Fig. 16(b). Observation of the results indicates that there exists little difference in the trend and final state between the elastic properties in the two transverse directions. In fact, the maximum relative difference between the two predicted tensile moduli for the constant and random fiber radii cases are 0.3% and 0.4% respectively.

3.2 Local Inelastic Behavior

Typically composite elastic properties are governed by the global homogenized stress/strain behavior, while inelastic behavior is governed at a smaller local scale where the presence of inclusions promote diffuse plastic flow. Although the homogenized global fields may be similar between two microstructures, due to the existence of peak stresses or strains in specific regions within the cross section, the inelastic behavior of the microstructures may promote drastic differences. Therefore, the effect of decreased spatial order on the local inelastic behavior of the composite was investigated using a similar technique applied in Section 3.1. For this analysis the matrix material was modeled as viscoplastic (as described in Section 2.2) in order to capture how the local variations in stress and strain fields alter the inelastic behavior of the composite as a function of spatial order. The viscoplastic constitutive relation applied to the matrix material within the FEM framework also allows for the effects of various loading rates to be studied in detail. Four strain rates (1E-3/s, 1E-2/s, 1E-1/s, and 1.00/s) were applied to three simulated microstructures (ordered, semi-random, and hard-core) and loaded in strain control for a total Cauchy strain of 1%.

Contours of the effective inelastic strain are presented for the ordered and hard-core distribution microstructures in Fig. 17 and Fig. 18 respectively for each of the four strain rates. It can be observed that the contour of inelastic strain resembles that of von Mises stress presented in Fig. 11. This intuitive similarity demonstrates the effect of fiber position variability on the concentration of stresses in regions with fibers aligned favorably with the loading direction and with small interfiber spacing, in addition to the subsequent inelastic behavior initiation and viscoplastic flow. The inelastic behavior of the ordered array (Fig. 17) retains a regular distribution, while the effective inelastic strain contours for the hard-core microstructure

(Fig. 18) demonstrates regions of significantly higher concentrations. The effect of strain rate can also be observed in the contours; as the loading strain rate decreases, the inelastic strains in the matrix increase as a result of the strain rate dependence included in the matrix constitutive relation. These results indicate the importance of accounting for fiber spatial variation when local inelastic behavior is of interest, especially at low strain rates. A qualitative observation of the contours reveals the possibility of under prediction in the magnitude of inelastic behavior in specific regions if a random microstructure was represented by an ordered array. These results merit additional investigation into the regions of high inelasticity concentrations to better understand the potential shortcomings involved in the simplification of random or experimental microstructures to regular fiber packing arrangements.

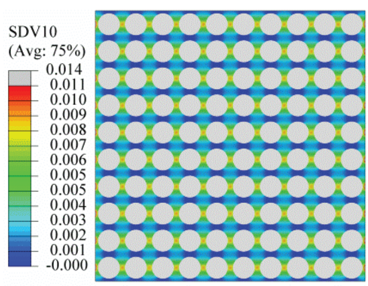

(a) $\dot{\varepsilon}_{11} = 1E-3/s$

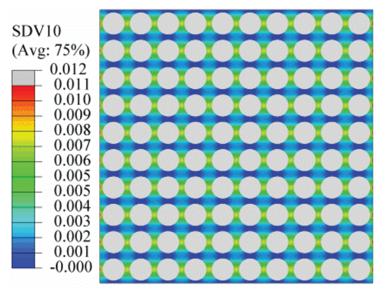

(b) $\dot{\varepsilon}_{11} = 1E-2/s$

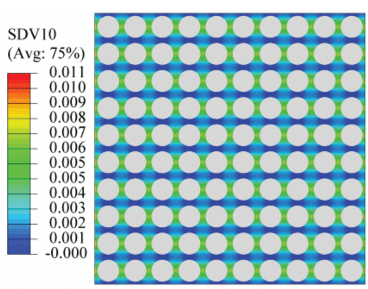

(c) $\dot{\varepsilon}_{11} = 1E-1/s$

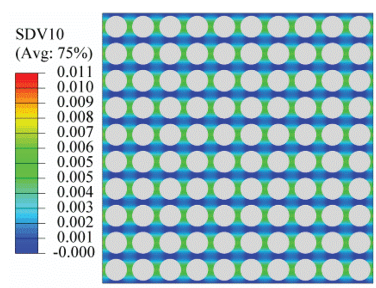

(d) $\dot{\varepsilon}_{11} = 1.00/s$

Figure 17: Effective inelastic strain contour for ordered RUC

Due to increase in inelastic material behavior concentrations observed for the random microstructures, the regions of maximum effective inelastic strain are investi-

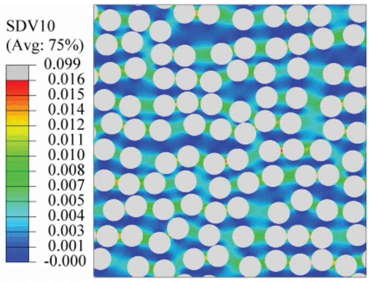

(a) $\dot{\varepsilon}_{11} = 1E-3/s$

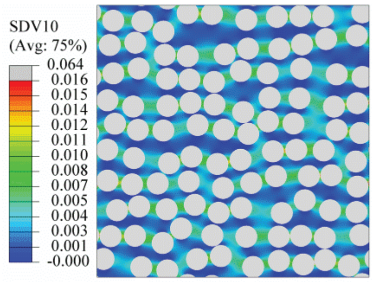

(b) $\dot{\varepsilon}_{11} = 1E-2/s$

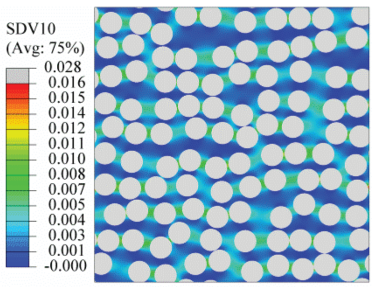

(c) $\dot{\varepsilon}_{11} = 1E-1/s$

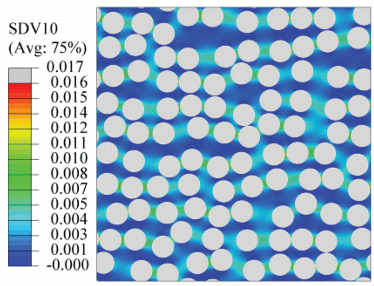

(d) $\dot{\varepsilon}_{11} = 1.00/s$

Figure 18: Effective inelastic strain contour for hard-core RUC

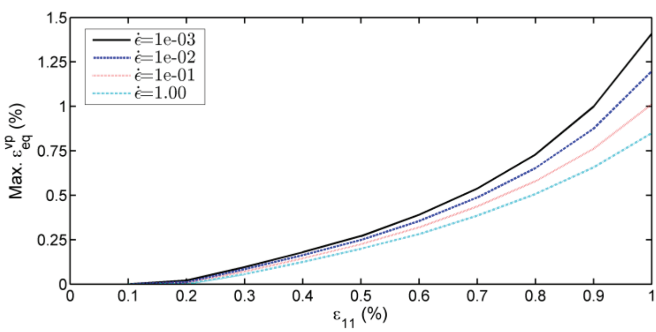

Figure 19: Maximum effective inelastic strain at four strain rates for an ordered microstructure

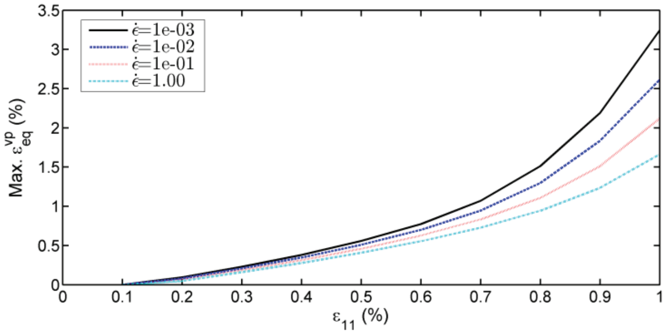

Figure 20: Maximum effective inelastic strain at four strain rates for a semi-random microstructure

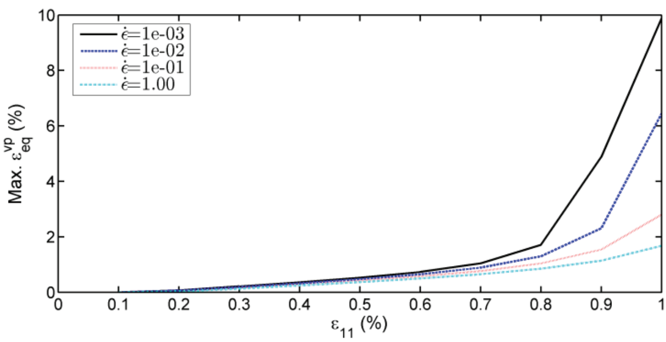

Figure 21: Maximum effective inelastic strain at four strain rates for a hard-core microstructure

gated in greater detail. This study is expected to further reveal the importance of accounting for architectural variation when accurately capturing the local inelastic behavior is necessary. The maximum effective inelastic (i.e., viscoplastic) logarithmic strain, ε_{eq}^{vp}, is plotted against the applied engineering strain, ε_{11}, for each of the four strain rates in Figs. 19, 20, and 21 for the ordered, semi-random, and hard-core microstructures respectively. The rate of effective inelastic strain, $\dot{e}_e^I$, for the associated flow rule [Goldberg, Roberts, and Gilat (2005)] is defined in Eqs.13 and14. The maximum values of effective inelastic strain, obtained through numerical integration of the effective inelastic strain rate, were extracted at each load increment to demonstrate the magnitude of local inelastic behavior as a function of strain rate and microstructural order. As the strain rate decreases for each of the three simulations, it can be observed that the maximum value of effective inelastic strain increases, similar to the qualitative results witnessed in Figs.17 and18. Addi-

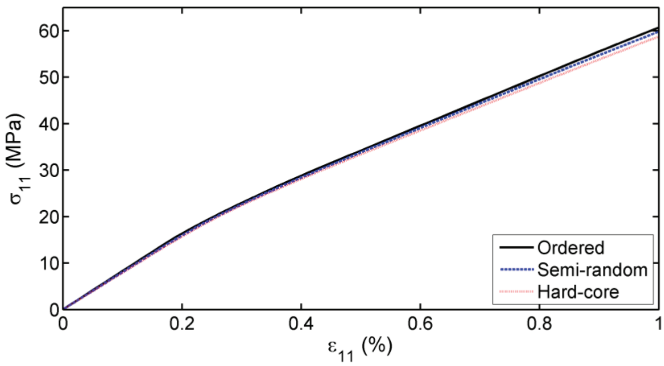

Figure 22: Cauchy stress vs. strain from three microstructures loaded at 1E-3/s strain rate

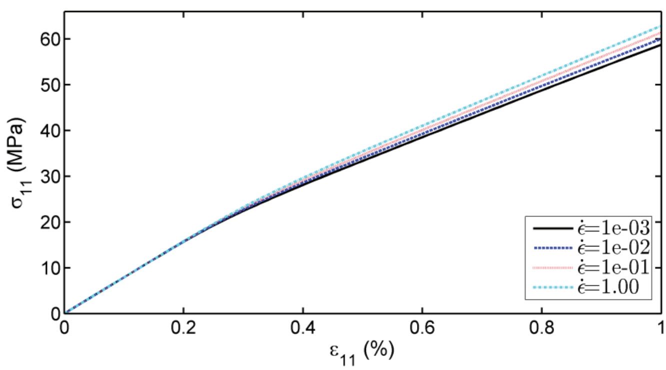

Figure 23: Cauchy stress vs. applied global strain for hard-core distribution at four strain rates

tionally, as the microstructures progress from ordered to hard-core, the maximum value increases drastically and the relative difference in the maximum values for the four strain rates also increases. This behavior is a result of the increase in stress concentration surrounding the fibers observed in Fig.11 caused by favorable fiber alignment with respect to loading direction and decreased interfiber spacing. The combination of stress concentrations and increased likelihood of resin rich pockets (i.e., particle free regions) promotes the initiation and unimpeded progression of viscoplastic matrix flow because the matrix is allowed to shear freely. Since the progression of inelastic material behavior is significant, investigations that simply quantify the inelastic behavior of ordered verses random microstructures using stress invariants, dilatational energy density, maximum stress and strain, or other elastic field variables to illustrate the increased likelihood of initiation [Wang et al. (2011); Huang, Jin, and Ha (2008); Trias et al. (2006); Maligno, Warrior, and Long (2009)] do not accurately characterize the more significant and pronounced effect of inelastic behavior progression as a function of increased loading.

After determining the local effect fiber position variability plays on the microscale inelastic fields, the focus now lies in how these fields are manifested at the macroscale. The global transverse Cauchy tensile stress versus strain responses of the ordered, semi-random, and hard-core composite microstructures are presented in Fig. 22 for a strain rate of 1E-3/s. At the global length scale it is observed that local inelastic phenomena have a minimal effect. In fact, at 1% strain the percent difference in predicted stress for the ordered and hard-core microstructures is only approximately 3.2%, a fairly insignificant amount. It is evident that as the loading applied to the composite RUCs is increased, the difference in predicted stress responses for the three microstructures also increases. Therefore, if a desired analysis involves large global strains, the effect of local inelastic events will play a more prominent role in the global composite behavior. Similarly, the stress versus strain response for the hard-core microstructure loaded in transverse tension with four strain rates is shown in Fig. 23. Comparing the results presented in Figs. 22 and 23, it is evident that strain rate plays a greater role in the global composite behavior than microstructural variability. Given the results for the local maximum inelastic strain magnitude and global inelastic stress versus strain behavior, the choice between explicitly analyzing an experimental or random microstructure or assuming order depends on the scale of interest, loading rate, and total applied strain.

3.3 Experimental versus simulated microstructures

The global and local effects of microstructural (i.e., fiber position) and geometric (i.e., fiber radius) variation have been demonstrated for the cases of elastic and inelastic material behavior and under various loading conditions (i.e., tensile and shear) and strain rates. The next logical step in the analysis involves quantifying the equivalence of the simulated disordered microstructures to those obtained from experimental micrographs. A set of criterion is developed in Liu and Ghoshal (2013a) that provides a systematic approach to determining statistical microstructure equivalence. The first step in the verification process involves simulating a random microstructure with an equivalent fiber volume fraction and fiber radius distribution. Next, the experimental and simulated RVEs must be sufficiently large such that the point processes have converged. Lastly, the point processes (e.g., Ripley's K-function) of the experimental and simulated microstructures must be compared for equivalence. If each of the criteria is satisfied within tolerance the microstructures can be regarded as statistically equivalent. An experimental and a simulated microstructure are presented in Fig. 24. Ripley's K-function was computed for both microstructures and plotted in Fig. 25. The apparent similarity between the two K-functions verifies the statistical equivalence of the experimental and simulated microstructures.

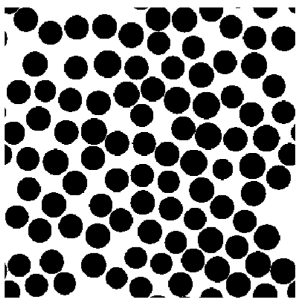

(a) Experimental microstructure

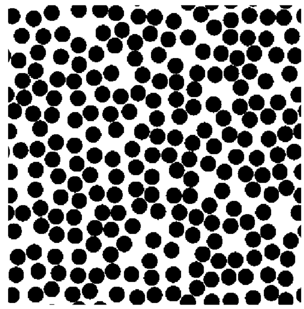

(b) Simulated microstructure

Figure 24: Microstructures for statistical equivalence verification

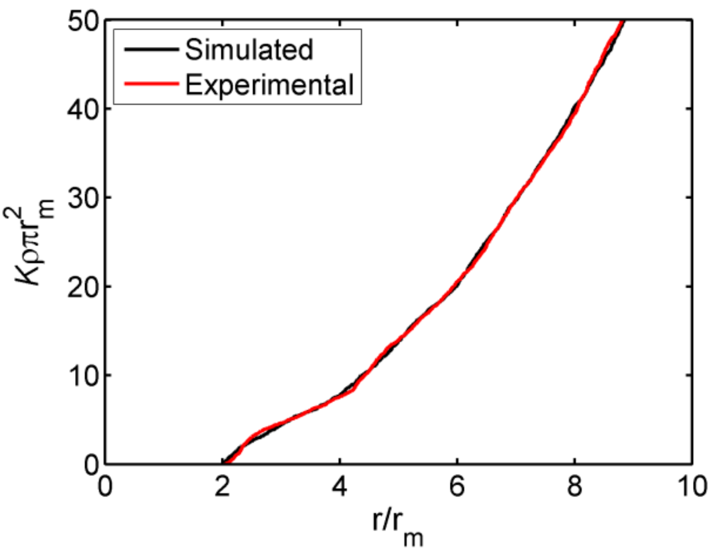

Figure 25: Experimental vs. simulated microstructure K-functions

Once the equivalence of experimental and generated microstructures is proven, one of the remaining questions is whether microstructures with identical K-functions have similar elastic behavior. The first step involved simulating multiple microstructures, each with 324 fibers, and comparing their respective K-functions. It was observed that the K-functions varied by less than 0.1% and had the same volume fractions and distributions for fiber radii; therefore, the microstructures can be considered statistically equivalent. Next, the microstructures were modeled in FEM as 3D triply periodic RUCs and an elastic analysis was run. The tensile moduli of the generated microstructures were then compared and found to be nearly identical. This comparison was repeated for 20 microstructures with similar results. These results indicate that the global elastic response of statistically equivalent microstructures, including those obtained from experimental micrographs, will also be equivalent.

Since it has been proven that statistical equivalence of microstructures (i.e., identical K-functions) is a good indication of global elastic behavior equivalence, another question that remains is whether the global inelastic behavior is also equivalent for two microstructures with identical K-functions. Two microstructures were simulated and their respective K-functions plotted for comparison, as seen in Fig. 26(a). The statistical equivalence of the two microstructures is evident. Using the FEM framework and viscoplastic constitutive model described previously, the two RUCs were simulated in transverse tension up to 1.45% Cauchy strain. The global stress vs. strain behavior of the two microstructures is plotted in Fig. 26(b). The mechanical behavior, including inelastic effects, is nearly identical for the two microstructures. These results imply that statistical equivalence of microstructures also can serve as in indication of equivalent mechanical behavior for both elastic and elastic/viscoplastic matrix behavior.

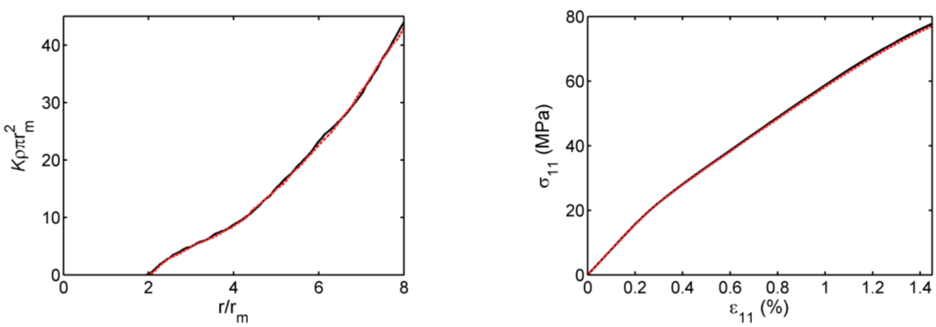

(a) K-function

(b) Stress vs. strain

Figure 26: Statistical and mechanical equivalence of two microstructures

An analysis was conducted to investigate whether convergence of the K-function can be correlated to a convergence in global elastic properties. In other words, the goal was to determine whether the elastic behavior of an experimental micrograph with a converged K-function remains stable as further variability is imposed. To provide insight into this question, an experimental microstructure was subjected to the Monte Carlo fiber position perturbation technique (i.e., experimental to hard-core) and simulated with the previously described FEM framework for tensile loading. The tensile modulus was plotted in Fig. 27. The relatively small decrease in tensile module (as compared with Fig. 9) and oscillations witnessed in the plot provide an indication that the elastic properties of the experimental microstructure are nearly stable. Therefore, it can be stated that convergence of the K-function provides a good indication of elastic property convergence.

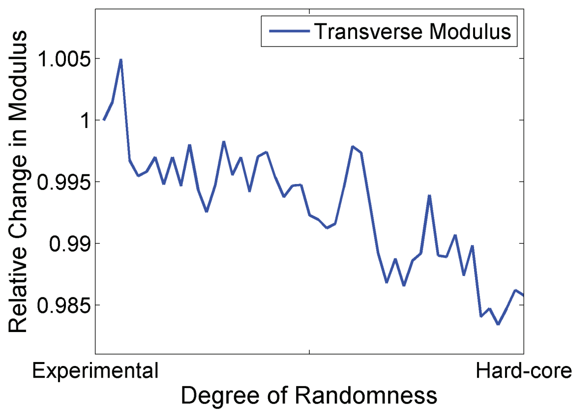

Figure 27: Relative tensile modulus vs. microstructural order (experimental to hard-core)

4 Conclusion

This paper presents a comprehensive investigation with the goal of quantifying the local and global effects of microstructural disorder using a 3D micromechanics-based, triply periodic FEM model. Studies were conducted over a variety of fiber arrangements progressing from ordered to hard-core for the purpose of linking the microscale variation and spatial randomness to the macroscale behavior of the composite. Architectural (e.g., fiber position) and geometric (e.g., fiber radius) variations as well as constituent constitutive behavior effects were investigated in detail for transverse loading of the composite microstructures. It was concluded that the importance of considering variations at the microscale depends greatly on the scale and phenomena of interest. For example, for a simple elastic analysis, the effects of microstructural variation are minimal when compared to those from material property or experimental uncertainty. Progressing from ordered to hard-core distributions, the authors saw a 5% decrease in the global tensile modulus and a 10% increase in shear modulus. However, if inelastic or small length scales are of interest the consideration of microscale variations becomes increasingly important for accurately capturing the localized stress concentrations and subsequent initiation and propagation of inelastic behavior. In fact, an 85% error in maximum effective inelastic strain would result from simplification of a hard-core microstructure to one that is ordered. Finally, the results were compared to experimental micrographs and it was concluded that the simulated and experimental microstructures can be considered experimentally equivalent and therefore will have similar mechanical behaviors, including inelastic.

Acknowledgement: This work is supported in part by the National Science Foundation Graduate Research Fellowship under Grant No. (2011124478), and Army Research Office under Grant No. (60766-EG), Program Manager Dr. Larry Russell. The authors would also like to thank Joseph Williams, undergraduate volunteer, Arizona State University, for his assistance in preprocessing the initial microstructures.

References

Abaqus (2009): Version 6.7, Abaqus/CAE and Abaqus/Explicit. Providence, RI: SIMULIA World Headquarters.

Bowden, P. B.; Jukes, J. A. (1972): The plastic flow of isotropic polymers. *Journal of Materials Science*, vol. 7, no. 1, pp. 52-63.

Buryachenko, V. A.; Pagano, N. J.; Kim, R. Y.; Spowart, J. E. (2003): Quantitative description and numerical simulation of random microstructures of composites and their effective elastic moduli. *International Journal of Solids and Structures*, vol. 40, no. 1, pp. 47-72.

Byström, J. (2003): Influence of the inclusions distribution on the effective properties of heterogeneous media. *Composites Part B: Engineering*, vol. 34, no. 7, pp. 587-592.

Chawla, N.; Chawla, K. K. (2006): Microstructure-based modeling of the deformation behavior of particle reinforced metal matrix composites. *Journal of Materials Science*, vol. 41, no. 3, pp. 913-925.

Danielsson, M.; Parks, D. M.; Boyce, M. C. (2002): Three-dimensional micromechanical modeling of voided polymeric materials. *Journal of the Mechanics* *and Physics of Solids*, vol. 50, no. 2, pp. 351-379.

Dong, L.; Atluri, S. N. (2012): Development of 3D Trefftz Voronoi Cells with Ellipsoidal Voids &/or Elastic/Rigid Inclusions for Micromechanical Modeling of Heterogeneous Materials. *CMC: Computers, Materials & Continua*, vol. 29, no. 2, pp. 169-212.

Dong, L.; Atluri, S. N. (2013): SGBEM Voronoi Cells (SVCs), with Embedded Arbitrary-Shaped Inclusions, Voids, and/or Cracks, for Micromechanical Modeling of Heterogeneous Materials. *CMC: Computers, Materials & Continua*, vol. 33, no. 2, pp. 111-154.

Dong, L.; Gamal, S. H.; Atluri, S. N. (2013): Stochastic Macro Material Properties, Through Direct Stochastic Modeling of Heterogeneous Microstructures with Randomness of Constituent Properties and Topologies, by Using Trefftz Computational Grains (TCG). *CMC: Computers, Materials & Continua*, vol. 37, no. 1, pp. 1-21.

Drugan, W. J.; Willis, J. R. (1996): A micromechanics-based nonlocal constitutive equation and estimates of representative volume element size for elastic composites. *Journal of the Mechanics and Physics of Solids*, vol. 44, no. 4, pp. 497-524.

Goldberg, R. K.; Roberts, G. D.; Gilat, A. (2005): Implementation of an associative flow rule including hydrostatic stress effects into the high strain rate deformation analysis of polymer matrix composites. *Journal of Aerospace Engineering*, vol. 18, no. 1, pp. 18-27.

Gusev, A. A. (1997): Representative volume element size for elastic composites: a numerical study. *Journal of the Mechanics and Physics of Solids*, vol. 45, no. 9, pp. 1449-1459.

Gusev, A. A.; Hine, P. J.; Ward, I. M. (2000): Fiber packing and elastic properties of a transversely random unidirectional glass/epoxy composite. *Composites Science and Technology*, vol. 60, no. 4, pp. 535-541.

Huang, Y.; Jin, K. K.; Ha, S. K. (2008): Effects of fiber arrangement on mechanical behavior of unidirectional composites. *Journal of Composite Materials*, vol. 42, no. 18, pp. 1851-1871.

Kanit, T.; Forest, S.; Galliet, I.; Mounoury, V.; Jeulin, D. (2003): Determination of the size of the representative volume element for random composites: statistical and numerical approach. *International Journal of Solids and Structures*, vol. 40, no. 13, pp. 3647-3679.

Kanouté, P.; Boso, D. P.; Chaboche, J. L.; Schrefler, B. A. (2009): Multiscale methods for composites: a review. *Archives of Computational Methods in Engi-*

neering, vol. 16, no. 1, pp. 31-75.

Krueger, R.; Paris, I. L.; Kevin O'Brien, T.; Minguet, P. J. (2002): Comparison of 2D FEM modeling assumptions with results from 3D analysis for composite skin-stiffener debonding. *Composite Structures*, vol. 57, no. 1, pp. 161-168.

Liu, K. C.; Arnold, S. M. (2013): Influence of Scale Specific Features on the Progressive Damage of Woven Ceramic Matrix Composites (CMCs). *CMC: Computers, Materials & Continua* vol. 35, no. 1, pp. 35-65.

Liu, K. C.; Ghoshal, A. (2013a): Validity of Random Microstructures Simulation in Fiber-reinforced Composite Materials. *Composites Part B: Engineering*, vol. 57, pp. pp. 56-70.

Liu, K. C.; Ghoshal, A. (2013b): Inherent symmetry and microstructure ambiguity in micromechanics. *Composite Structures*, vol. 10, no. 8, February 2014, pp. 311-318.

Maligno, A. R.; Warrior, N. A.; Long, A. C. (2009): Effects of inter-fibre spacing on damage evolution in unidirectional (UD) fibre-reinforced composites. *European Journal of Mechanics-A/Solids*, vol. 28, no. 4, pp. 768-776.

Melro, A. R.; Camanho, P. P.; Pinho, S. T. (2008): Generation of random distribution of fibres in longfibre reinforced composites. *Composites Science and Technology*, vol. 68, no. 9, pp. 2092-2102.

Ostoja-Starzewski, M. (1998): Random field models of heterogeneous materials. *International Journal of Solids and Structures*, vol. 35, no. 19, pp. 2429-2455.

Pae, K. D.; Mears, D. R. (1968): The effects of high pressure on mechanical behavior and properties of polytetrafluoroethylene and polyethylene. *Journal of Polymer Science Part B: Polymer Letters*, vol. 6, no. 4, pp. 269-273.

Pugh, H. L. D.; Chandler, E. F.; Holliday, L.; Mann, J. (1971): The effect of hydrostatic pressure on the tensile properties of plastics. *Polymer Engineering & Science*, vol. 11, no. 6, pp. 463-473.

Pyrz, R. (1994): Quantitative description of the microstructure of composites. Part I: Morphology of unidirectional composite systems. *Composites Science and Technology*, vol. 50, no. 2, pp. 197-208.

Rabinowitz, S.; Ward, I. M.; Parry, J. S. C. (1970): The effect of hydrostatic pressure on the shear yield behaviour of polymers. Journal of Materials Science, vol. 5, no. 1, pp. 29-39.

Ripley, B. D. (1977): Modelling spatial patterns. *Journal of the Royal Statistical Society. Series B (methodological)*, pp. 172-212.

Reddy, J. N. (1987): A generalization of two-dimensional theories of laminated composite plates. *Communications in Applied Numerical Methods*, vol. 3, no. 3, pp. 173-180.

Romanov, V.; Lomov, S. V.; Swolfs, Y.; Orlova, S.; Gorbatikh, L.; Verpoest, I. (2013): Statistical analysis of real and simulated fibre arrangements in unidirectional composites. *Composites Science and Technology*, vol. 87, pp. 126-134.

Sab, K. (1992): On the homogenization and the simulation of random materials. *European Journal of Mechanics. A. Solids*, vol. 11, no. 5, pp. 585-607.

Shan, Z.; Gokhale, A. M. (2002): Representative volume element for non-uniform micro-structure. *Computational Materials Science*, vol. 24, no. 3, pp. 361-379.

Smit, R. J. M.; Brekelmans, W. A. M.; Meijer, H. E. H. (1999): Prediction of the large-strain mechanical response of heterogeneous polymer systems: local and global deformation behaviour of a representative volume element of voided polycarbonate. *Journal of Mechanics and Physics of Solids,* vol. 47, no. 2, pp. 201–221.

Socrate, S.; Boyce, M. C. (2000): Micromechanics of toughened polycarbonate. *Journal of Mechanics and Physics of Solids,* vol. 48, no. 2, pp. 233–273.

Swaminathan, S.; Ghosh, S.; Pagano, N. J. (2006): Statistically equivalent representative volume elements for unidirectional composite microstructures: Part I-Without damage. *Journal of Composite Materials*, vol. 40, no. 7, pp. 583-604.

Terada, K.; Hori, M.; Kyoya, T.; Kikuchi, N. (2000): Simulation of the multi-scale convergence in computational homogenization approaches. *International Journal of Solids and Structures*, vol. 37, no. 16, pp. 2285-2311.

Torquato, S. (2001): Random heterogeneous materials: microstructure and macroscopic properties (Vol. 16). Springer.

Trias, D.; Costa, J.; Turon, A.; Hurtado, J. E. (2006): Determination of the critical size of a statistical representative volume element (SRVE) for carbon reinforced polymers. *Acta Materialia*, vol. 54, no. 13, pp. 3471-3484.

Wang, Z.; Wang, X.; Zhang, J.; Liang, W.; Zhou, L. (2011): Automatic generation of random distribution of fibers in long-fiber-reinforced composites and mesomechanical simulation. *Materials & Design*, vol. 32, no. 2, pp. 885-891.

Ward, I. M.; Sweeney, J. (2012): Mechanical properties of solid polymers. Wiley.

Whitney, W.; Andrews, R. D. (1967): Yielding of glassy polymers: volume effects. *Journal of Polymer Science. C*, vol. 16, pp. 2981-2990.

Wongsto, A.; Li, S. (2005): Micromechanical FE analysis of UD fibre-reinforced composites with fibres distributed at random over the transverse cross-section. *Composites Part A: Applied Science and Manufacturing*, vol. 36, no. 9, pp. 1246-1266.

Wronski, A. S.; Pick, M. (1977): Pyramidal yield criteria for epoxides. *Journal of Materials Science*, vol. 12, no. 1, pp. 28-34.